*J. Fluid Mech.* (1980), *vol.* 100, *part* 2, *pp.* 243–255
*Printed in Great Britain*



# Exploratory temperature-tagging measurements of turbulent spots in a heated laminar boundary layer

By C. W. VAN ATTA† AND K. N. HELLAND

Institute for Pure and Applied Physical Sciences and
Department of Applied Mechanics and Engineering Sciences,
University of California, San Diego, La Jolla, California 92093

(Received 23 April 1979 and in revised form 17 January 1980)

Exploratory measurements to study transport mechanisms in turbulent spots have been made using a passive temperature-tagging technique. Temperature fluctuations were measured on the centre-plane of spots artificially generated in the laminar boundary layer on a fully heated flat plate. The fluid near the wall is cooled and fluid far from the wall is heated during passage of the spot, with a more complex behaviour at intermediate locations. Contours of ensemble-averaged temperature disturbance measured relative to the laminar undisturbed profile show a region of maximum heating near the upper front of the spot and a region of maximum cooling at the rear of the spot near the wall, a structure strongly anti-correlated with corresponding contours of the longitudinal velocity disturbance as measured by Zilberman, Wygnanski & Kaplan (1977). The observed position of the upper heating maximum appears to be related to mean streamline pictures obtained by previous investigators in which streamlines entering the rear of the spot are deflected upward into the heated region. In conical similarity co-ordinates there is a near coincidence of the maxima and minima in the temperature disturbance contours with the two stable foci, or points of accumulation, for particle paths found by Cantwell, Coles & Dimotakis (1978), but the position of the hot core region cannot be explained in terms of the centre-line particle paths. An alternate viscosity-dependent scaling produces closer coincidence of the temperature and velocity disturbance extrema with the foci.

## 1. Introduction

Recent measurements of the structure of turbulent spots in a flat plate boundary layer by Wygnanski, Sokolov & Friedman (1976; hereinafter referred to as WSF), Cantwell, Coles & Dimotakis (1977; referred to as CCD), and others have raised a number of questions about the mechanism by which a turbulent spot mixes boundary-layer fluid to transfer momentum and scalar properties during transition. Velocity measurements have thus far not provided a full picture of the paths of fluid particles mixed by the vigorous turbulent diffusion within the spot. It seems reasonable to think that tagging parts of the fluid with a passive scalar, like heat, could eventually shed some light on this question. In a recent study of the large-scale structure of a fully turbulent boundary layer, Chen & Blackwelder (1978) produced the desired temperature contamination by heating the ceiling of their wind tunnel. Here, we

† Also: Scripps Institution of Oceanography.

0022–1120/80/4530–1930 $02.00 

report the initial results of an adaptation of a similar technique to study the structure of turbulent spots. The entire surface of a flat plate is uniformly heated, producing a laminar velocity and temperature field of well-known form in which artificially generated turbulent spots may develop. Neglecting the molecular diffusion of heat, the fluid particles are labelled with a temperature corresponding to their vertical, or $y$, location, but with no information concerning their origin in $x$ or $z$. The present results for the temperature field on the centre-line of the spot do not, therefore, directly give information on individual particle paths within the spot. We find that the temperature measurements do, however, provide some insight into the structure and mixing processes within the spot, which complements previous velocity measurements. The temperature contours directly suggest a structure consistent with the presence of vortical regions of fluid accumulation within the spot. Since the temperature field is a scalar quantity, the form of the deduced structure is invariant under Galilean transformation. It is thus not subject to the same ambiguities in interpretation noted for stream-function measurements by previous workers, who found that the overall structural pattern obtained was strongly sensitive to the convection speed assumed.

## 2. Experimental arrangement

The measurements were made in the low-speed, low-turbulence, closed-circuit wind tunnel in the Department of Applied Mechanics and Engineering Sciences at the University of California, San Diego. The test section is 76 cm wide, 9·8 m long, and nominally 76 cm high. The Plexiglas ceiling of the test section is mounted on jacks to allow adjustment of the pressure gradient. The basic experimental set-up was very similar to that employed by Wygnanski *et al.* (1976). A 1·27 cm thick machined flat aluminium plate was mounted horizontally in the mid-plane of the test section, with the leading edge of the plate 24 cm downstream of the end of the contraction. The leading edge of the plate was machined to a wedge angle of 30°, rounded off at the apex. The angle of attack of the plate, after final adjustment by means of levers connected to the rods supporting the plate from below, was less than 1° relative to the free-stream direction. The pressure gradient was estimated from measurements of the free-stream acceleration to be on the order of $(2/\rho U_\infty^2)\,dp/dx \simeq 1{\cdot}6 \times 10^{-4}\ \mathrm{cm}^{-1}$, where $x$ is the downstream distance from the leading edge. The plate was heated by 0·1 mm thick Sierracin heating pads bonded to the bottom of the plate. For the experiments to be described here, the power supplied to the heaters was fixed by the available laboratory supply voltage and produced a plate surface temperature $\theta_w$ of 100–110 °C at the measurement stations. Using the largest possible passive heating optimizes the signal-to-noise ratio for the temperature measurements. Comparison of the present results with the later data of Antonia *et al.* (1980) obtained in the same experimental apparatus using much weaker heating ($\Delta\theta = \theta_w - \theta_\infty \approx 10$ °C) indicates that for all the measurements the temperature acted as a passive scalar, consistent with the small value of $Gr/Re^2 \approx 10^{-3}$. Here, the Grashof number $Gr = g\delta^3\Delta\theta/\nu^2\theta_\infty$, where $\delta$ is the boundary-layer thickness and $\nu$ is the kinematic viscosity, and the Reynolds number $Re = U_\infty\delta/\nu$. Near the leading edge the plate surface temperature increased monotonically with $x$, reaching a nearly constant value downstream of $x = 57$ cm. In the latter region, temperature variations of 2–3 per cent were measured

in both $x$ and $z$, with larger decreases in temperature occurring only within the thermal boundary layers at the tunnel walls and near the trailing edge.

The probe-traversing mechanism was mounted on horizontal rails connected to the outside of the tunnel and allowed adjustment of the probe location in three co-ordinate directions. The probes were attached to an airfoil-shaped strut connected to a traversing mechanism through sealed slots in the tunnel side wall. The vertical location of the hot and cold wires relative to the plate was determined optically by sighting on the wires and their reflexions in the polished aluminium plate with a travelling telescope-cathetometer stage.

Laminar mean velocity and temperature profiles $u_l(y)$ and $\theta_l(y)$ measured at the two downstream stations were in good agreement with the results of laminar boundary-layer theory for the velocity and temperature fields, as calculated by Blasius and Pohlhausen, respectively (e.g. Schlichting 1968, p. 280).

The spot-producing spark was generated between the tips of two sewing needles mounted in an insulating plug at $x = x_s = 29$ cm from the leading edge of the plate in the centre-plane of the tunnel. The spanwise ($z$) separation of the needles was about 2 mm, and they protruded about 1 mm into the boundary layer. Spots were generated at a rate of 3 per second using a square-wave generator to trigger a capacitor discharge ignition system as in the experiments of WSF.

Velocity measurements were made with linearized DISA 55M10 constant-temperature anemometers and platinum hot wires 2·5 $\mu$m in diameter and 1 mm long. Temperature was measured with a constant current d.c. bridge which supplied a current of 64 $\mu$A to a platinum cold wire 0·6 $\mu$m in diameter. The lengths of the cold wires employed ranged from 0·6 to 1·1 mm.

For the initial turbulent spot experiments reported here, only the spot temperature was measured as the relatively large heating $\theta_w - \theta_\infty = \Delta\theta \sim 80$ °C) would have required large corrections for the effect of temperature fluctuations on the hot-wire response. Simultaneous measurements of both velocity and temperature have recently been made with much smaller heating ($\Delta T \sim 10$ °C) and will be reported in the future. Analog recordings of the temperature signals on the spot centre-line for 500 consecutive spots were made on the plate (and spot) centre-line at about 25 $y$ positions across the boundary layer. Data were obtained for two values of the free-stream velocity $U_\infty$ and for two stations 104·7 cm and 135 cm downstream of the leading edge. The square-wave trigger signal for the spark was also recorded on the analog tape and was used as a trigger for the digitizing operation. Following a fixed time delay after each spark, 2048 digital samples were taken for each spot temperature signature $\theta(t)$ at a sample rate of 10000 Hz. These data were then ensemble-averaged over 400 spots for each of the 2048 sample times to produce ensemble-averaged mean-temperature signatures $\overline{\theta}(t; y)$ for each value of $y$. The difference $\Theta(t; y) = \overline{\theta}(t; y) - \theta_l(y)$, where $\theta_l(y)$ is the steady laminar boundary-layer value, represents the ensemble-mean temperature disturbance produced by the passage of the 400 spots. For each spot the turbulent fluctuation around the ensemble mean is defined as $\theta(t; y) - \overline{\theta}(t; y)$ and has an ensemble-mean value of zero. The r.m.s. ensemble-averaged value of this fluctuation, $\theta'(t; y)$, was calculated for each sampling time $t$. This furnished a measure of the variation over different spots used in the ensemble average, which may be interpreted as a turbulent intensity relative to the ensemble mean.

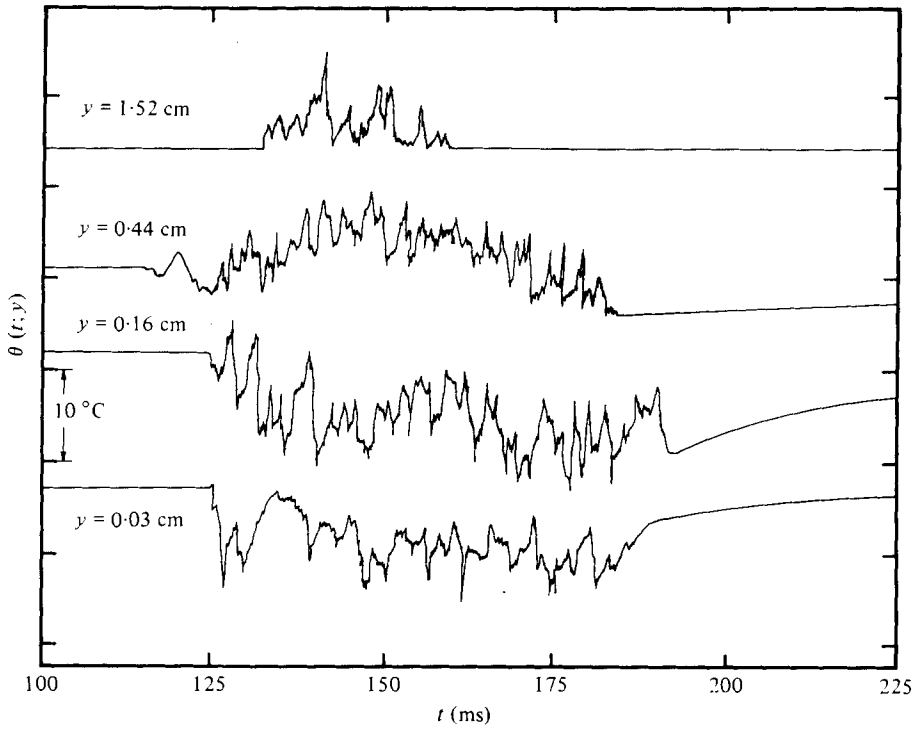


FIGURE 1. Representative individual spot temperature *versus* time traces for several heights in boundary layer. $U_\infty = 8{\cdot}6$ m s$^{-1}$, $x = 135$ cm, $\Delta\theta = 80$ °C.

## 3. Results

Some individual spot temperature signals are shown for several values of $y$ in figure 1 and corresponding ensemble averages $\bar{\theta}$ and $\theta'$ are shown in figures 2 and 3. Relative to the undisturbed laminar temperature profile, the outer part of the spot is associated with a heating of the flow in which the temperature perturbation reaches a maximum somewhat before half of the elapsed time of passage of the spot at each $y$ location. This maximum is progressively delayed further in time as the wall is approached. The central part of the spot is characterized by an initial brief cooling, followed by a positive perturbation several times longer in duration, then a larger cooling followed by a relaxation back to the ambient value. The minimum ensemble-averaged temperature $\bar{\theta}$ occurs at the trailing turbulent–laminar interface of the spot. Close to the wall the temperature perturbation is negative throughout. A very steep initial cooling is followed by a further gradual decrease in temperature (preceded by a plateau for the smallest values of $y$) which reaches a minimum at the trailing interface of the spot, after which the temperature relaxes back to the laminar value.

The $\theta'(t; y)$ traces generally show a very sharp increase to a maximum value at the front of the spot, followed by rapid decrease to a plateau value persisting throughout most of the remaining duration of the disturbance. The maximum in $\theta'$ always occurs simultaneously with the largest gradient in the corresponding ensemble average, irrespective of the sign of this gradient. To determine whether the maximum value near the leading edge could be due to jitter in the arrival time of the spots at the

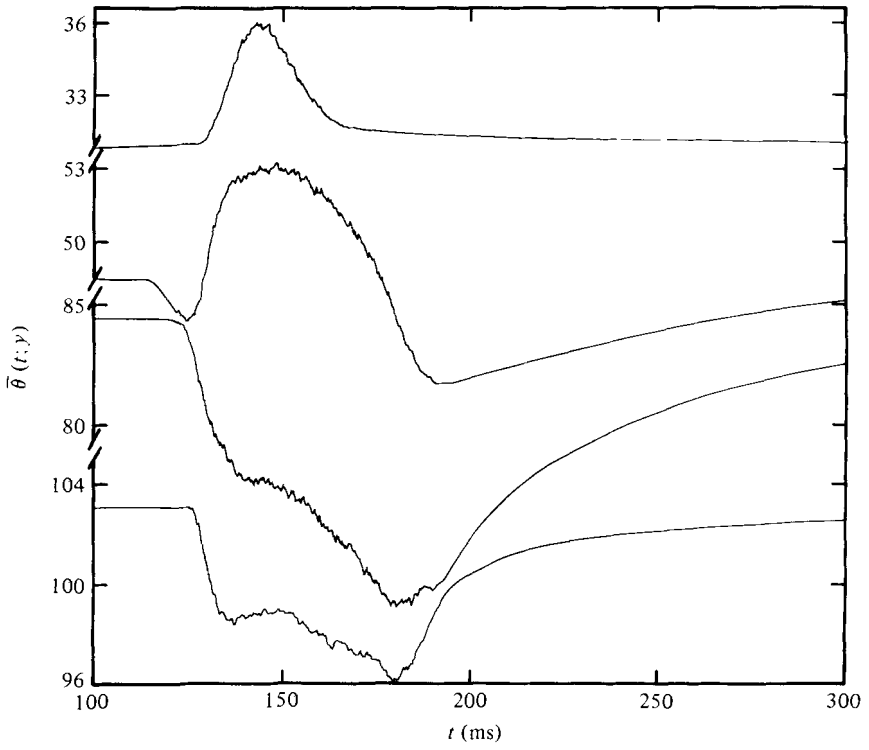


FIGURE 2. Ensemble-averaged mean-temperature traces $\bar{\theta}(t;y)$ for 400 spots. $U_\infty = 8{\cdot}6$ m s$^{-1}$, $x = 135$ cm, $\Delta\theta = 80$ °C.

measuring station, the data were reprocessed, performing the ensemble-averaging relative to the leading edge of the spot rather than with respect to the spark discharge. The leading edge was detected using the absolute value of the time derivative $d\theta/dt$ for discrimination. The results were not sensitive to the value chosen for discrimination, and a final value equal to $d\theta/dt = 3{\cdot}76 \times 10^3$ °C s$^{-1}$ was used for comparison with the spark-averaged data. The data for $\theta'$ obtained in this way were practically identical with those obtained by averaging relative to the spark, even in the leading-edge region. The jitter in arrival time of the spot thus did not contribute measurably to $\theta'$. One could argue that if there is a meaningful mean-level signal signature for each spot realization, then it would be useful to measure fluctuations relative to this level, which would be obtained by application of a suitable low-pass filter. We chose not to do this, as our experience with the present data and that of others (I. Wygnanski, private communication) with similar data indicated that the contribution of the 'fluctuations' to the total signal probably could not be unambiguously separated from the mean when defined in this manner.

Averaging with respect to the leading edge considerably sharpened the gradients in the ensemble mean near the leading edge, without changing its mean position. The interface gradients produced by this kind of averaging were much larger than those obtained averaging relative to the spark. However, because the initial changes in temperature at the interface for different spots were with high probability of the same sign and relatively large, the ensemble mean also invariably exhibited a

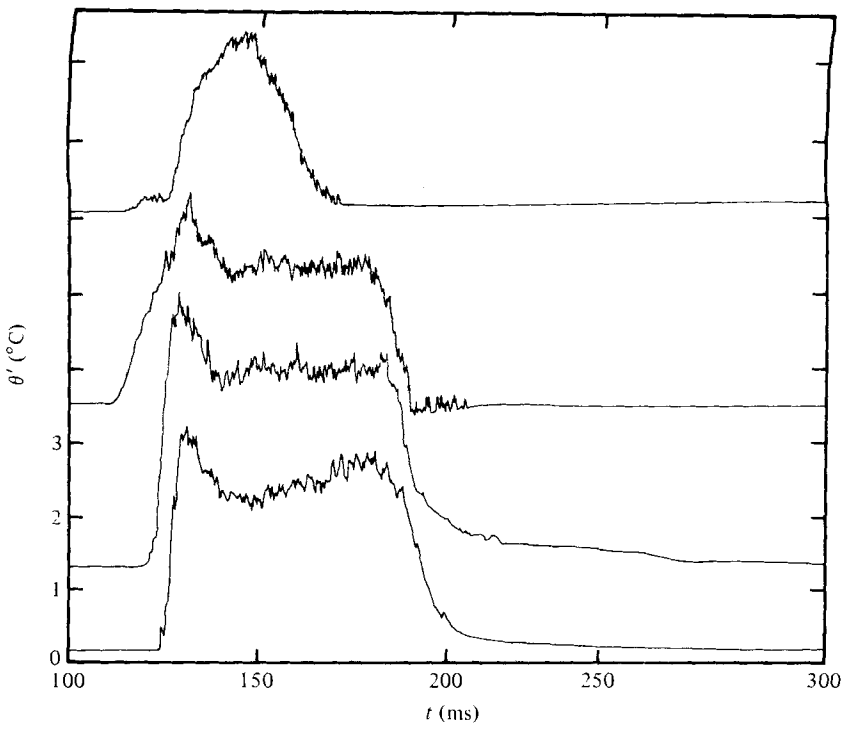


FIGURE 3. Ensemble-averaged turbulent temperature fluctuations $\theta'(t;y)$ for 400 spots. $U_\infty = 8{\cdot}6$ m s$^{-1}$, $x = 135$ cm, $\Delta\theta = 80$ °C.

pronounced bump or spike (depending on the time scale of observation) resembling an overshoot of the mean value. Since only the initial fluctuations upon encountering the interface were coherent, and automatically lined up by the discrimination procedure, only a single spike appeared, and the mean then immediately settled down to the value obtained by averaging with respect to the spark. Similar behaviour has been noted by Antonia *et al.* (1980) for both velocity and temperature data. As the bump appears to be an artifact of the sampling method, and the effect on the overall temperature contours is minor, we present here only the data obtained averaging relative to the spark. There is in some cases near the wall evidence of a second weaker local maximum of $\theta'$ near the rear of the spot. Since the averaging was performed relative to the spark discharge, the longer time delays and larger dispersion in arrival times associated with the trailing edge of the spots will produce a greater underestimation of the magnitude of gradients in $\overline{\theta}$ and $\theta'$ at the trailing edge than at the leading edge. This is probably the source of the relatively slowly varying tails noticeable in some of the $\theta'$ data at the trailing edge as may be observed in the lower trace in figure 3. Outside the spot $\theta'$ returns to the free-stream temperature fluctuation level of $\theta'/\Delta\theta \simeq 0{\cdot}2\,\%$.

An example of the overall two-dimensional ensemble-averaged temperature structure on the spot centre-line is shown in the contour plots of $\Theta(t)$ in figures 4 and 5. There is a temperature perturbation maximum (heating) in the outer part of the spot which arrives first, followed by a minimum (cooling) near the wall near the back of the spot. The positive slope of the contour lines above the negative minimum is asso-

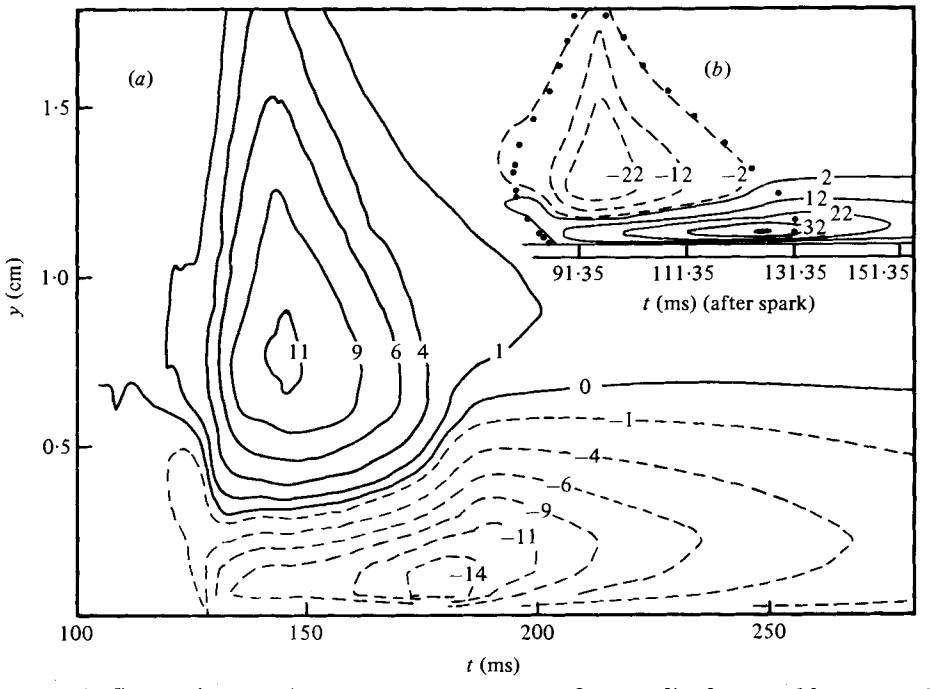


FIGURE 4. Space–time equi-temperature contours of normalized ensemble-averaged mean-temperature and velocity perturbations relative to laminar boundary-layer values. (*a*) Present results for $\Theta(t,y)/\Delta\theta$. Contour labels give value of $\Theta/\Delta\theta \times 10^2$ and $u/U_\infty \times 10^2$. $U_\infty = 8{\cdot}6$ m s$^{-1}$, $x = 135$ cm, $\Delta\theta = 80$ °C. (*b*) Results of Zilberman *et al.* (1977) for velocity perturbation $u(t,y)/U_\infty$. Contour labels refer to percentage of $U_\infty$. $U_\infty = 10$ m s$^{-1}$, $x = 70$ cm, $\Delta\theta = 0$. ●, mean spot interface position.

ciated with the occurrence of maximum negative temperature perturbations just preceding the trailing interface as noted previously. Near the wall a tongue of relatively cold fluid protrudes out from the wall at the front of the spot. This feature occurs in the same region as the strong negative vertical velocity ($v$) with maximum negative value occurring on the leading edge, as found by WSF (their figures 22 and 23) both on the centre-line and for all lateral ($z$) stations. The cooling in this region is thus largely due to the downward transport of colder, slower-moving fluid from larger values of $y$ by the laminar flow field perturbations generated ahead of the spots. As illustrated in figure 4, there is a one-to-one correspondence of all these features with the contour lines of constant $u$-component velocity disturbance from laminar values as measured by Zilberman *et al.* (1977). Comparing these two figures, we see that relative to the laminar boundary-layer values a temperature excess is always associated with a velocity deficit and a temperature deficit is always associated with a velocity excess, i.e. the two fields are strongly anti-correlated.

This anti-correlation is to be expected in general because in the original undisturbed laminar boundary layer there is a one-to-one correspondence between the temperature of a fluid particle and its velocity, i.e. the higher-temperature fluid near the wall has a lower velocity and as the free stream is approached the temperature decreases while the velocity increases.

The observed location of the heating maximum in the upper forward portion of

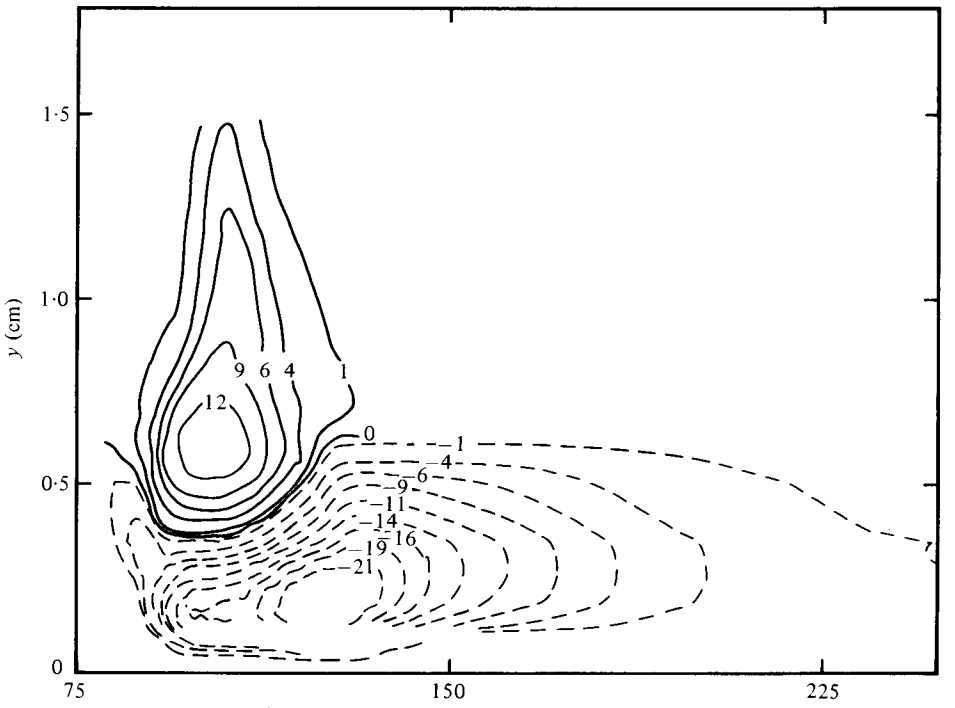


FIGURE 5. Contour map of $\Theta(t, y)/\Delta\theta$. $U_\infty = 8{\cdot}6$ m s$^{-1}$, $x = 104{\cdot}7$ cm, $\Delta\theta = 80$ °C.

the spot, which must be due to upward transport of hotter fluid, bears a qualitative resemblance with the streamline contours obtained by CCD (their figures 16 and 17) for a reference frame moving at a speed equal to $0{\cdot}78U_\infty$ and with those of WSF (their figure 25) for a frame moving at a speed of $0{\cdot}9U_\infty$. Above a certain value of $y$, streamlines entering the rear of the spot then bend upward, rising to their maximum height in the region corresponding to our heating maximum. In the CCD data, there is also a contribution from streamlines entering the front of the spot near the wall, which then bend abruptly upward into the region of the heating maximum. Since the streamline picture obtained is a sensitive function of the convection velocity chosen for presentation, more detailed comparison with the temperature data may be unwarranted. For example, most of the upward-bending streamlines just referred to in the CCD data appear to originate in the outermost part of the laminar boundary layer where the temperature is nearly equal to $\theta_\infty$, a feature which can be altered by choosing a different convection speed. There is a weak suggestion from the streamline data for smaller $y$ values of some downward transport of colder fluid into the rear of the spot which might be associated with the observed cooling maximum near the wall at the back of the spot.

The cooling contours protruding outward near the wall at the front of the spot can be understood in the streamline context as due to the downward flow produced at the front of the spot by the vortex structure which is obtained when using a convection velocity equal to that of the spot leading edge (e.g. WSF, figure 25).

A contour plot of the r.m.s. temperature fluctuation $\theta'(y, t)$ is shown in figure 6.

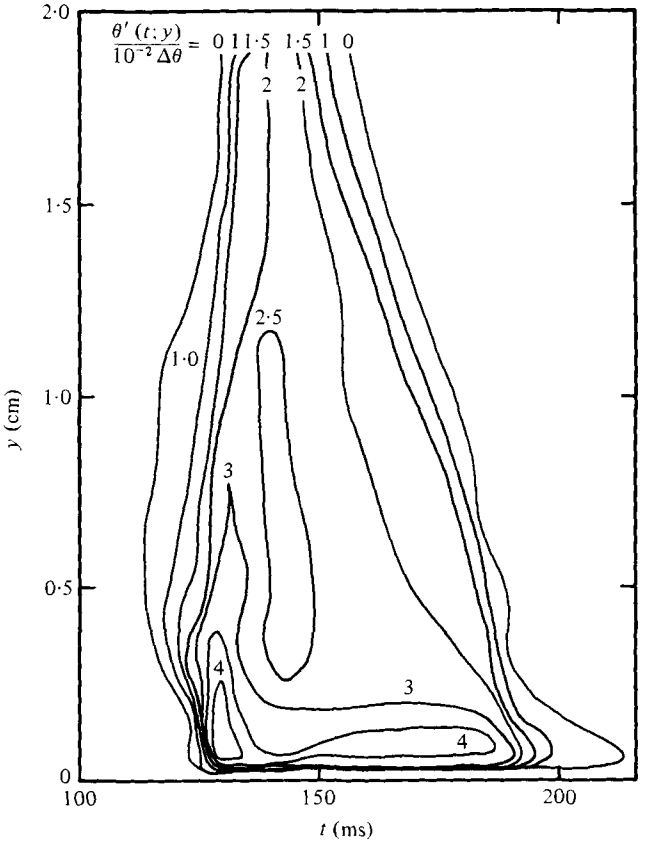


FIGURE 6. Contour map of normalized temperature fluctuation relative to ensemble mean $\theta'(t, y)/\Delta\theta$. $U_\infty = 8{\cdot}6$ m s$^{-1}$, $x = 135$ cm, $\Delta\theta = 80$ °C. Contour labels give value of $(\theta'/\Delta\theta) \times 10^2$.

The largest fluctuation levels occur in a narrow region near the wall extending from a maximum near the front of the spot to the rear of the spot, and including the 'cold spot' near the trailing interface. For $y$ locations below the upper 'hot spot' region of closed temperature perturbation contours, the largest fluctuations occur near the leading edge of the spot. Elsewhere in the interior the fluctuation level is fairly uniform. In the outer part of the spot the maximum temperature fluctuation occurs closer to the centre of the spot.

Contour plots were constructed for the $\theta(t, y)$ and $\Theta(t, y)$ data in terms of the conical similarity variables $\xi$ and $\eta$ introduced by CCD, where $\xi = (x - x_0)/U_\infty(t - t_0)$ and $\eta = y/U_\infty(t - t_0)$, and $x_0$ and $t_0$ were obtained by the graphical procedure of CCD using arrival times for the front and back interfaces of the spot. One might expect the non-dimensional temperature field $\bar{\theta}/\Delta\theta$ to exhibit conical similarity to a degree similar to that found for the non-dimensional stream function $\psi/U_\infty^2(t - t_0)$ by CCD. The present data for only two stations in $x$ were inadequate for a conclusive test of conical similarity. The two sets of contours did appreciably collapse toward one another, but definitive comparison is hampered by the lack of distinguished structure in the contours, which are only mildly undulating and exhibit no closed contours. The temperature perturbation contours measured relative to laminar values at the

same values of $y$ do possess distinguishing features, but the perturbation would not be expected to obey conical similarity since the laminar field possesses a different similarity, governed by molecular diffusion of heat and momentum. However, similarity contour plots of these data may be useful in identifying and locating corresponding features in temperature and velocity fields, and these are presented in figure 7. The position $(\xi, \eta)$ of the heating maximum in the upper front of the spot is nearly the same at the two stations, and thus follows the conical similarity fairly well. The $\xi$ co-ordinate of the cooling maximum near the wall is invariant, but $\eta$ changes appreciably, as do the overall sizes of the heating and cooling regions. Compared with the velocity data, the stream-function contours of CCD exhibit a primary vortex in the outer part of the spot at nearly the same values of the $\xi, \eta$ co-ordinates as the perturbation heating maximum we find. The stream-function results produced no vortical region corresponding to our cooling maximum near the wall. However, since the stream-function picture obtained is strongly dependent on the convection velocity adopted in the analysis of CCD, it cannot be strictly compared with our measured temperature (scalar) field contours, which are independent of the speed of a uniformly moving observer. Alternatively, comparison can be made with the particle trajectories computed by CCD, which, as they point out, are also independent of the speed of a uniformly moving observer. This comparison is made in figure 8. There is an interesting correspondence between the particle path pattern and the temperature contours. The maxima and minima of $\Theta(\xi, \eta)$ appear to be associated with the two stable foci, or points of accumulation, found by CCD. The $\xi$ locations of both foci correspond closely to the $\xi$ co-ordinates of the maxima and minima of $\Theta$. The $\eta$ co-ordinates of both foci are about 50 % larger than those of the maximum and minima of $\Theta$. However, in $\xi, \eta$ co-ordinates the overall height of the spot as defined by our 1 % $\Theta/\Delta\theta$ contour is considerably larger than that of the CCD spot. Recalling that the CCD measurements were made in a fluid with lower kinematic viscosity ($H_2O$), the differences in $\eta$ scaling suggested that replacing the $y$ scaling of the conical similarity approximation with a viscosity-dependent $y$ scaling might improve the agreement. As first noted by Schubauer & Klebanoff (1956), the spot thickness increases approximately with distance like a fully developed turbulent boundary layer with an initial thickness equal to that of the laminar layer at the position of the spark, i.e.

$$\delta_t = 0{\cdot}37(x - \hat{x}_0)^{\frac{4}{5}} (\nu/U_\infty)^{\frac{1}{5}},$$

where $\hat{x}_0 = x_s - 2{\cdot}72 x_s^{\frac{5}{8}} (\nu/U_\infty)^{\frac{3}{8}}$, obtained by equating the turbulent boundary-layer thickness $\delta_t$ to the laminar boundary-layer thickness $\delta_l = 5{\cdot}2(\nu x/U_\infty)^{\frac{1}{2}}$ at the spark location $x_s$. The dimensionless $y$ co-ordinate is then

$$\eta^* = y/\delta_t = 2{\cdot}7y(x - \hat{x}_0)^{\frac{4}{5}} (U_\infty/\nu)^{\frac{1}{5}}.$$

The values of $\hat{x}_0$ for the present data and that of CCD are 20·5 cm and 8·57 cm, respectively. The $\eta^*$ values of the upper heating maximum for the present temperature data and for the upper focus of the CCD velocity data are found to be 0·26 and 0·24, respectively, in much closer agreement than the corresponding values of $\eta$ (0·0065 and 0·0038, respectively). The value of $\eta^*$ for both the cooling maximum and lower focus of CCD is 0·045, as compared with the corresponding values of $\eta$ of 0·0008 and 0·0006, respectively. Thus, the $(\xi, \eta^*)$ locations of CCD loci and our $\Theta$ extrema are in close agreement. A recent extensive experimental test of the $(\xi, \eta^*)$ co-ordinate

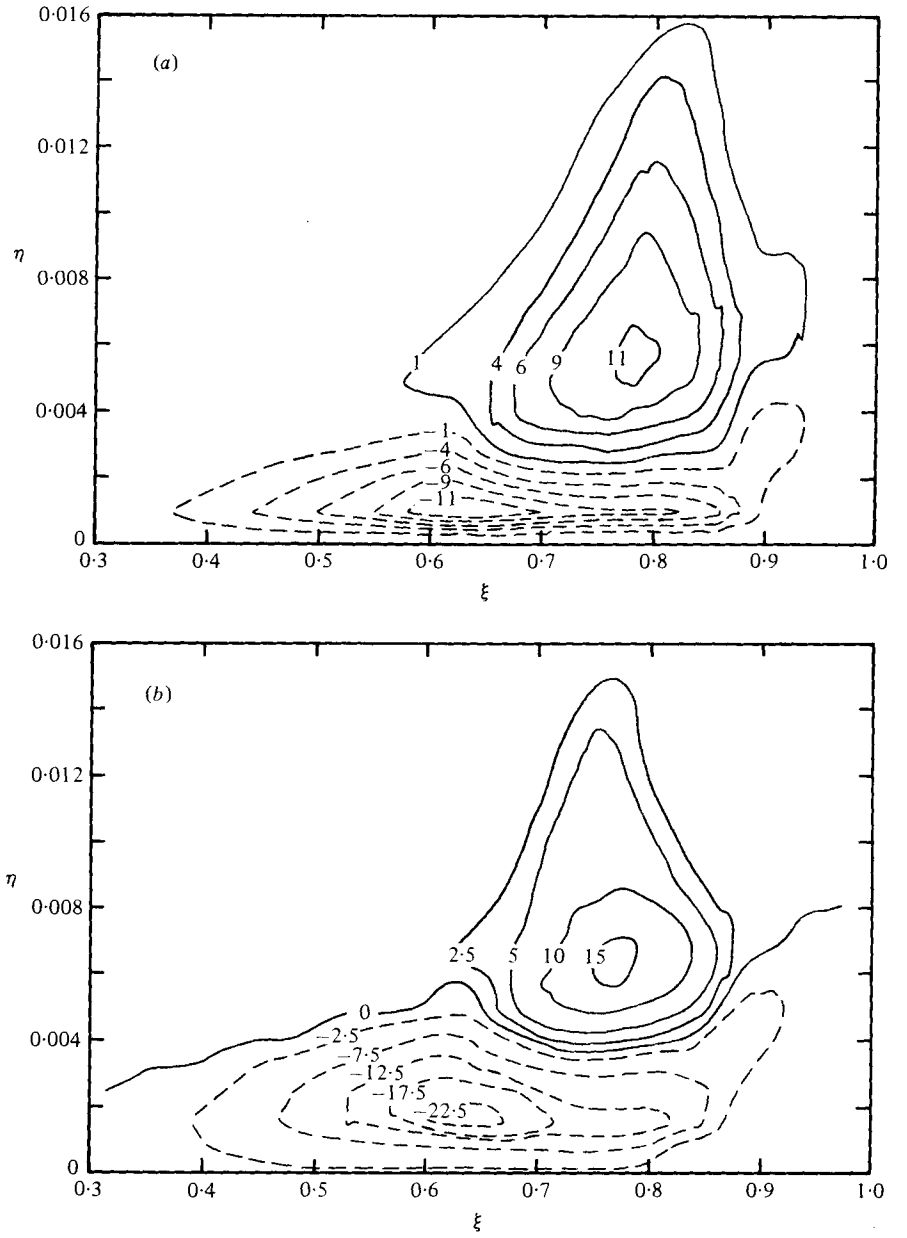


FIGURE 7. Replot of the data of figures 4 and 5 in conical similarity co-ordinates,

$$\xi = (x-x_0)/U_\infty(t-t_0), \quad \eta = y/U_\infty(t-t_0).$$

$x_0 = 29$ cm, $t_0 = -12$ ms. (*a*) $x = 135$ cm, $U_\infty = 8{\cdot}6$ m s$^{-1}$, $\Delta\theta = 80$ °C. (*b*) $x = 104{\cdot}7$ cm, $U_\infty = 8{\cdot}6$ m s$^{-1}$, $\Delta\theta = 80$ °C.

transformation at the University of Southern California has shown that the values of $\xi$ and $\eta^*$ associated with the maximum positive and negative longitudinal velocity perturbations are Reynolds-number dependent (I. Wygnanski, private communication). For a comparable Reynolds number ($Re_\delta = 4963$, air) the $(\xi, \eta^*)$ values of the

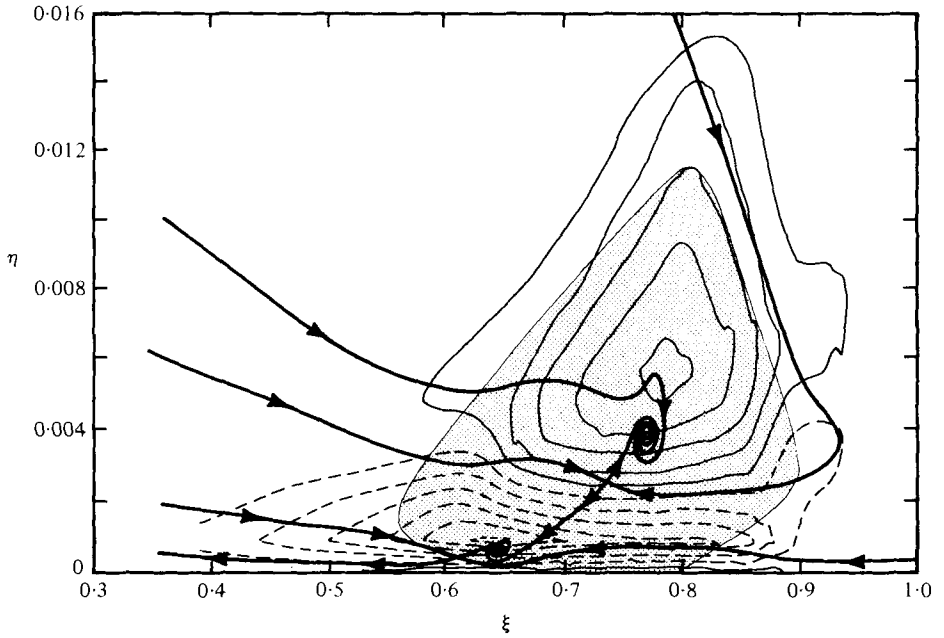


FIGURE 8. Comparison of temperature perturbation contours of figure 7(*a*) with particle path trajectories computed by Cantwell *et al.* (1978). For CCD data, $U_\infty = 0{\cdot}59$ m s$^{-1}$, $x = 119$ cm; the working fluid was water.

velocity perturbation maxima are in close quantitative agreement with the corresponding $\Theta$ extrema of the present data ($Re_\delta = 4690$), as qualitatively observed in figure 4(*a*), and hence are also in close agreement with the $(\xi, \eta^*)$ co-ordinates of the corresponding foci of the CCD data ($Re_\delta = 4360$). Here, $Re_\delta = U_\infty \delta_l / \nu$, where $\delta_l$ is the laminar boundary-layer thickness at the measurement station. For the CCD data, one does not know presently if the $(\xi, \eta^*)$ foci co-ordinates will correspond to actual points of accumulation for particle paths in $\xi, \eta^*$ co-ordinates. A calculation of particle paths in $(\xi, \eta^*)$ co-ordinates would be a useful contribution at this point. The $(\xi, \eta^*)$ transformation has also been suggested and developed independently by M. Sokolov (private communication), for application to simultaneous temperature and velocity turbulent spot data of Antonia *et al.* (1980).

Conclusions regarding the possible connexion between the mean particle paths and the temperature field must be made with caution. As pointed out by CCD, turbulent dispersion may cause the mean of an ensemble of particle paths through a given initial point to be quite different from the particle paths computed from the mean-velocity field (Hunt & Mulhearn 1973). Also, information solely from the centre-line of the spot may produce misleading results for quantities sensitive to the effects of three-dimensional transport from lateral positions. From the comparison in figure 8, the position of the upper hot-core region cannot be explained in terms of the centre-line particle paths. The fluid near the heating maximum must come from positions closer to the wall, whereas the mean particle paths converging in the upper focus originate in unheated regions behind the spot and outside the laminar boundary layer. Perhaps the near coincidence of the upper hot core with the upper focus is purely accidental. The position of the lower cooling maximum is compatible with the particle paths

associated with entrainment in the rear of the spot and coming from cooler regions at larger values of $y$. However, some particles also arrive in this region from hotter regions nearer the wall ahead of the spot.

## 4. Conclusions

Contours of ensemble-averaged temperature disturbance measured relative to the laminar undisturbed profile show a region of maximum heating near the upper front of the spot and a region of maximum cooling at the rear of the spot near the wall, a structure strongly anti-correlated with corresponding contours of the longitudinal velocity disturbance as measured by Zilberman *et al.* (1977). The observed position of the upper heating maximum appears to be related to mean streamline representations obtained by previous investigators, in which streamlines entering the rear of the spot are deflected upward into the heated region. In conical similarity co-ordinates there is a near coincidence of the maxima and minima in the temperature disturbance contours with the two stable foci, or points of accumulation, for particle paths found by Cantwell *et al.* (1978), but the position of the hot core region cannot be explained in terms of the centre-line particle paths computed from the ensemble mean velocity.

This work was supported by NSF Grant ENG78-25088. We thank Michael Head and Richard Stout for help with the data processing, Dr John LaRue for loan of the cold-wire temperature bridge, and Prof. I. Wygnanski for useful criticism and for sending us a draft manuscript describing a test of viscosity-dependent scaling. A short account of this work (Van Atta & Helland 1980) was given at the IUTAM Symposium on Laminar–Turbulent Transition.

## REFERENCES

Antonia, R. A., Chambers, A. J., Sokolov, M. & Van Atta, C. W. 1980 Simultaneous temperature and velocity measurements in the plane of symmetry of a transitional turbulent spot. *J. Fluid Mech.* (to appear).

Cantwell, B., Coles, D. & Dimotakis, P. 1978 Structure and entrainment in the plane of symmetry of a turbulent spot. *J. Fluid Mech.* **87**, 641–672.

Chen, C. P. & Blackwelder, R. F. 1978 Large-scale motion in a turbulent boundary layer: a study using temperature contamination. *J. Fluid Mech.* **89**, 1–31.

Hunt, J. C. R. & Mulhearn, P. J. 1973 Turbulent dispersion from sources near two-dimensional obstacles. *J. Fluid Mech.* **61**, 245–274.

Schlichting, H. 1968 *Boundary Layer Theory*, 6th edn, pp. 280–281. McGraw-Hill.

Schubauer, G. B. & Klebanoff, P. S. 1956 Contributions on the mechanics of boundary-layer transition. *N.A.C.A. Rep.* no. 1289.

Van Atta, C. W. & Helland, K. N. 1980 Temperature tagging measurements of turbulent spots in a heated laminar boundary layer. *Proc. IUTAM Symp. on Laminar–Turbulent Transition, Univ. of Stuttgart, Sept.* 1979. Springer.

Wygnanski, I., Sokolov, M. & Friedman, D. 1976 On the turbulent 'spot' in a boundary layer undergoing transition. *J. Fluid Mech.* **78**, 785–819.

Zilberman, M., Wygnanski, I. & Kaplan, R. E. 1977 Transitional boundary layer spot in a fully turbulent environment. *Phys. Fluids Suppl.* **20**, 258–271.